Advances in Concrete Construction, *Vol. 4, No. 3 (2016) 173-194*
DOI: http://dx.doi.org/10.12989/acc.2016.4.3.173

Numerical study of a new constructive sequence for movable scaffolding system (MSS) application

José Ramón Díaz de Terán[*1], Vladimir Guilherme Haach[2a], José Turmo[3b] and Juan José Jorquera[4c]

[1]*Departamento de Estruturas, Universidade de Sao Paulo, Brasil*
[2]*Departamento de Estruturas, Universidade de Sao Paulo, Brasil*
[3]*Departamento de Ingeniería de la Construcción, Universidad Politécnica de Cataluña, Spain*
[4]*Departamento de Ingeniería Minera, Geológica y Cartográfica, Universidad Politécnica de Cartagena, 30202 Cartagena, Murcia, Spain*

(Received June 4, 2016, Revised December 14, 2016, Accepted December 15, 2016)

Abstract. This paper consists in a study of a new contructive sequence of road viaducts with Movable Scaffolding System (MSS) using numerical tools based on finite element method (FEM). Traditional and new sequences are being used in Spain to build viaducts with MSS. The new sequence permits an easier construction of one span per week but implies some other issues related to the need of two prestressing stages per span. In order to improve the efficiency of the new sequence by reducing the number of prestressing stages per span, two solutions are suggested in this study. Results show that the best solution is to introduce the 100% of the prestressing force at the self-supporting core in order to improve the road viaduct construction with movable scaffolding system by reducing execution time without increasing economic costs.

Keywords: movable scaffolding system; span by span casting; loop joint; critical path; transverse deflection; prestressing stage; self-supporting core

1. Introduction

The constructive process of viaducts with movable scaffolding system (MSS) is one of the most sophisticated as it involves the utilization of one auxiliary and movable provisional structure (Daebritz and Lee 2010). The movable scaffolding system (MSS) has been used since the sixties. The first time this construction system was used was in Germany: the Krahnember Viaduct, designed by Hans Wittfoht was built in 1961 (Leonhardt 1994). Mainly after the seventies its use spread over Europe.

The use of MSS is recommended when environmental criteria imply not to affect the ground or

∗Corresponding author, Ph.D., E-mail: jringcamjunior@gmail.com
[a]Professor
[b]Professor
[c]Lecturer

http://www.techno-press.org/?journal=acc&subpage=7 ISSN: 2234-0912 (Print), 2234-179X (Online)

(a) Phase (b) Phase 2

Fig. 1 Traditional sequence

(a) Phase 1 (b) Phase 2

Fig. 2 New sequence

if the topography should be overcome. Nevertheless the cost of this constructive sequence is high enough to be only affordable when the number of spans is equal or greater than 5 (Díaz de Terán, *et al.* 2016).

As of modern requirements of Health and Safety at work (Council 1989, Council 1992), MSS allows the use of collective security measures. Operational risks are lower than with other constructive methods. In order to guarantee the security, MSS requires a specific project where calculation basis of the scaffolding, loads and combinations that have been considered should be detailed (Kwak and Son 2006).

Recently, some improvements and advances have been carried. Organic prestress permits saving material and reducing stresses in the structure (Pacheco *et al.* 2011). Also, it implies a significant advance regarding environmental and sustainability requirements (Pacheco *et al*. 2009).

Nowadays two different procedures to construct viaducts with MSS have been applied in Spain (Díaz de Terán *et al.* 2016). The first procedure is called traditional sequence (Fig. 1) and consists in a first casting phase that is formed by the lower slab and webs and a second casting phase that is formed by the top slab of the box girder. Once the first and second casting phases are completed, the total prestressing force (100%) is introduced. The second procedure is called new sequence (Fig. 2) and consists in a self-supporting core that is formed by the lower slab, webs and top slab cantilevers and a second casting phase that is formed by the central zone of the top slab. Once the self-supporting core is completed, a partial prestressing force is introduced, so that the scaffolding can advance to the next span.The traditional and new sequences are described by Díaz de Terán (Díaz de Terán *et al.* 2016, Díaz de Terán 2013, Díaz de Terán *et al.* 2013 a, b).

The new sequence has three main issues (Díaz de Terán *et al.* 2016):

• Extraction of the inner formwork is difficult unless loop joints are used at the casting joint between phases, loop joints depend on the bond transverse reinforcement (Zwicky 2013 a, b, Shin *et al.* 2016). The use of loop joints has been proposed in order to avoid this issue (Díaz de Terán 2013, Díaz de Terán *et al.* 2013 a, b).

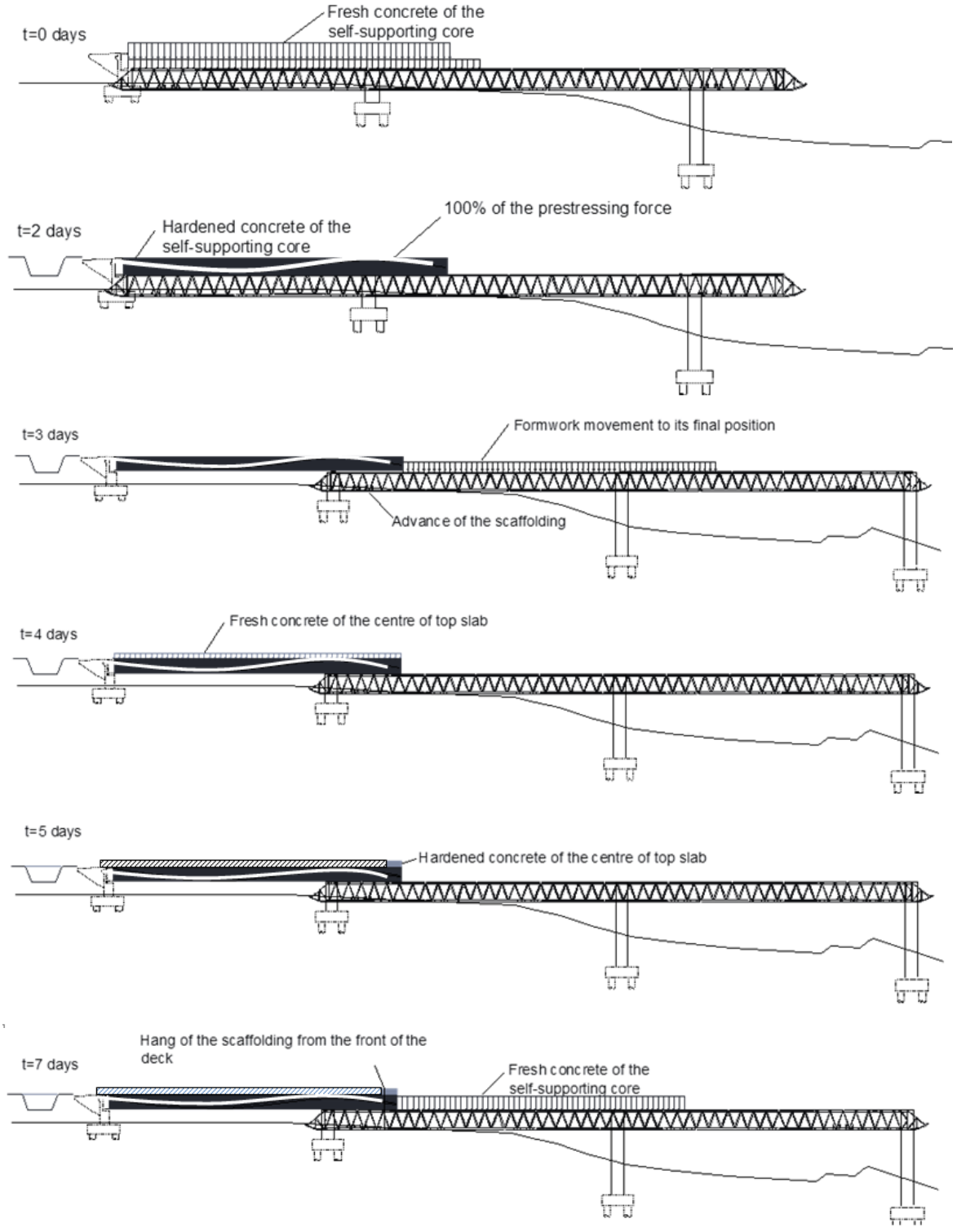

Fig. 3 Solution 1: 100% of prestressing force at the self-supporting core

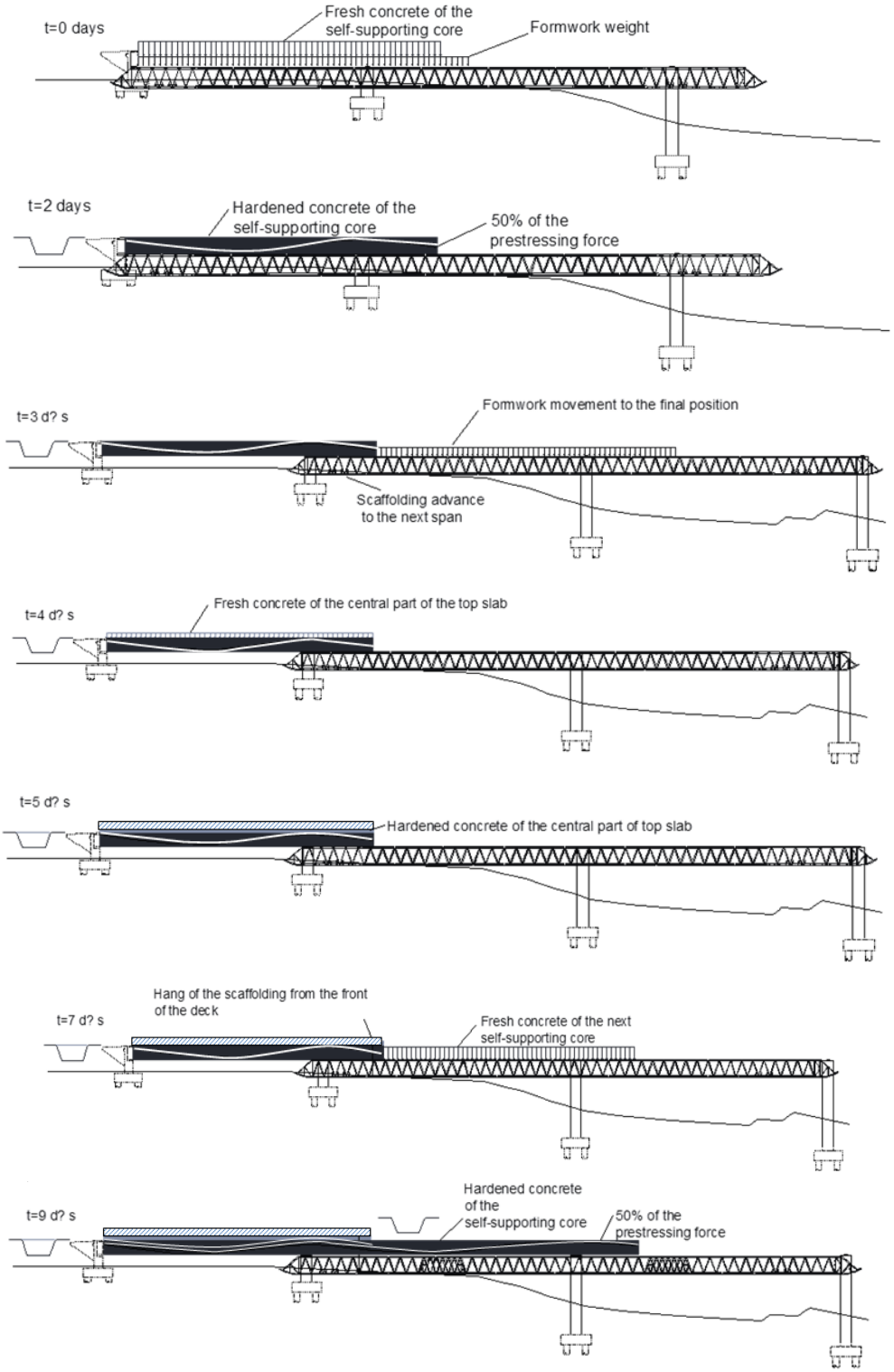

Fig. 4 Solution 2: 50% of prestressing forcé at the self-supporting core

• The necessity of stiffening elements to prevent the transverse deflection of the self-supporting core (Díaz de Terán *et al.* 2016).

• The necessity of two prestressing stages for each span (Díaz de Terán *et al.* 2016).

In this paper, "Solution 1" and "Solution 2" are the second and third variations of the new sequence respectively. They are suggested to avoid the problem of two prestressing stages per span and reduce them to only one.

Solution 1

Solution 1 consists in introducing 100% of the total prestressing force into the self-supporting core. The Solution 1consists of several stages (Fig. 3):

1) t=0 days: The scaffolding supports the weight of the formworks and fresh concrete of the self-supporting core.

2) t=2 days: The concrete of the self-supporting core has hardened and 100% of the prestressing force is introduced.

3) t=3 days: The scaffolding moves to its new position at the next span.

4) t=4 days: The fresh concrete of the central part of the top slab is placed.

5) t=5 days: The concrete of the central part of the top slab has hardened.

6) t=7 days: The scaffolding hangs from the front of the deck and fresh concrete of the next self-supporting core is placed.

Solution 2

The Solution 2 consists in the use of tendons that cross two spans and that are partially prestressed at 50% when each self-supporting core is constructed. When the section is completed and the self-supporting core of the next span is constructed, the prestressing force of the section reaches the 100% of the total prestressing force. The stages of this solution are (Fig. 4) are:

1) t=0 days: The scaffolding supports the weight of the formworks and fresh concrete of the self-supporting core.

2) t=2 days: The concrete of the first casting span has hardened and a partial prestressing of 50% is introduced so that the self-supporting core is created.

3) t=3 days: The scaffolding moves to its position at the next span.

4) t=4 days: The fresh concrete of the central part of the top slab is placed.

5) t=5 days: The concrete of the central part of the top slab has hardened.

6) t=7 days: The scaffolding hangs from the front of the deck and fresh concrete of the next self-supporting core is placed.

7) t=9 days: When the concrete of the next self-supporting core has hardened, a tendon that crosses the last two spans is prestressed at 50% of the total force, so that the previous span reaches 100% of prestressing force and the current self-supporting core reaches 50% of the total force.

Therefore, this study aims to compare and discuss the structural behaviour both in Ultimate

Fig. 5 Longitudinal viaduct geometry. Grey colour: standard sections. White colour: transition sections

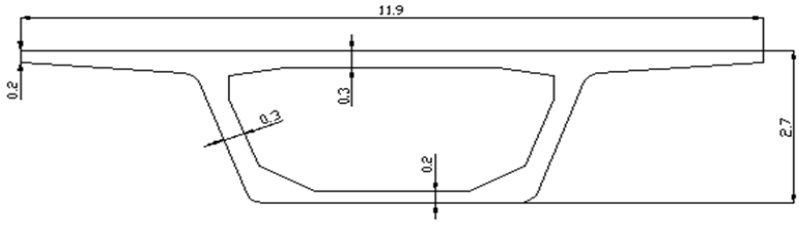

Fig. 6 Standard section

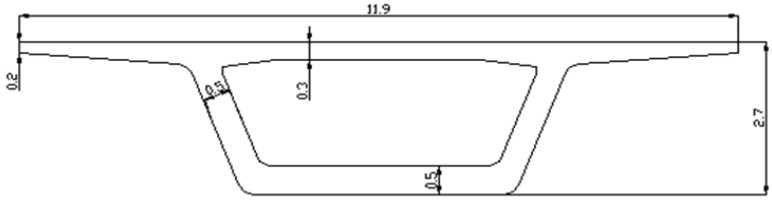

Fig. 7 Transition section

Table 1 Mechanical characteristics of each section type depending on the constructive sequence

	Traditional sequence		New sequence	
	Standard section	Transition section	Standard section	Transition section
1st phase area (m^2)	2.80	4.16	5.74	7.11
Total area (m^2)	6.80	8.17	6.80	8.17
1st phase inertia (m^4)	1.35	1.65	5.85	7.35
Total inertia (m^4)	6.56	8.45	6.56	8.45
Gravity centre 1st phase (m)	0.76	0.71	1.66	1.46
Gravity centre total (m)	1.79	1.59	1.79	1.59

Limit State (U.L.S) and Service Limit State (S.L.S) of the 4 constructive sequences for road viaducts named: traditional sequence, new sequence, solution1 and solution 2. The main parameter considered here is the percentage of the prestressing force introduced at the first casting phase. It should be pointed that tendon layout and total prestressing force are identical for all considered construction procedures. The prestressing force at the first casting phase of traditional sequence is 100%, while at the first casting phase of new sequence, Solution 1 and Solution 2 prestressing force is 75%, 100% and 50% respectively. Different aspects have been studied in this paper:

1) The distribution of global bending moments at different phases;

2) The distribution of internal forces at different elements of the section with special attention on the casting joint elements;

3) The distribution of stresses and crack opening in the cross-section in order to assure durability (Sadeghi and Rezvani 2013, Bojidar 2015).

4) The transversal deformation of the self-supporting core in the new sequence, solution 1 and solution 2.

2. Model description

The numerical model applied to study the new constructive sequence of road viaducts with Movable Scaffolding System (MSS) was defined using the software Midas Civil. Two different numerical models were developed to perform this study: a 2D model, to evaluate the global distribution of bending moments; and a 3D model to conduct analysis of stresses, strains and cracking on the cross section of the bridge. Calculations have been performed with Multifrontal Sparse Gaussian Analysis (Liu 1992, Duff and Reid 1984, Demmel *et al.* 1999). The tolerance that has been considered in 2D models and 3D models was 5% and 1%, respectively.

2.1 Geometric and mechanical characterization of the viaduct

A common bridge configuration contructed in Spain with typical cross section and active reinforcement has been selected to perform the numerical study. Nine spans have been considered in Finite Element Models. The external span length was 42 m. while the internal span length was 55 m (Fig. 5). Only the box girder has been modelled. Abutments and piers have been replaced by supports that will be described at the boundary conditions.

The bridge span consisted in a single cell box girder. The total height of the bridge span was 2.7 m. The wings were cantilevers of 2.6 meters and they had a variable thickness between 20 and 39 cm. The lower slab width was 4.5 m. Total width was 11.9 m.

Bridge span was divided longitudinally in two different sections, the first one (standard section) was placed at the middle of the spans and the second one (transition section) was placed over the bents. In standard section webs had a thickness of 30 cm and the lower slab had a thickness of 20 cm, see Fig. 6. In transition section the lower slab and webs had a thickness of 50 cm, see Fig. 7. 2D and 3D F.E. models have considered these two sections.

Geometrical characteristics during the constructive process depended on the constructive sequence (Table 1). If the traditional sequence was considered, the first casting phase consisted in the lower slab and the webs. On the other hand, if the new sequence, Solution 1 or Solution 2 were considered, the first casting phase consisted in a self-supporting core formed by the lower slab, webs and cantilevers of the top slab.

2D models were constituted by standard Timoshenko beam elements of Midas Civil (Midas Civil 2011) of 0.5 m length. Tendon position over piers was over the gravity centre of the section in order to induce a positive moment to compensate the moments due to the permanent loads.

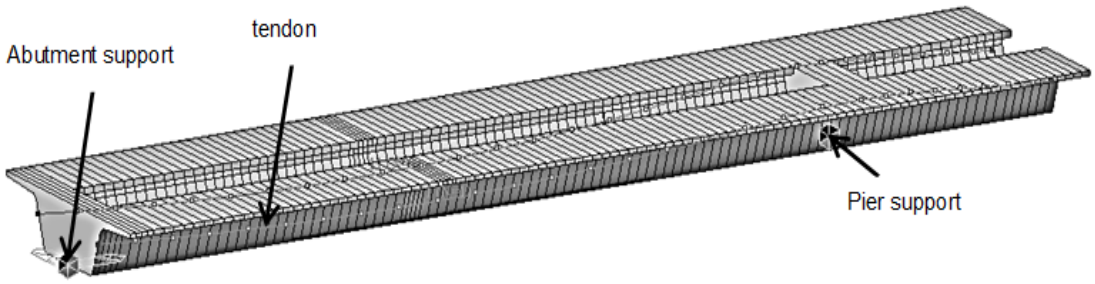

Fig. 8 Tendon positions in first casting phase of the first span

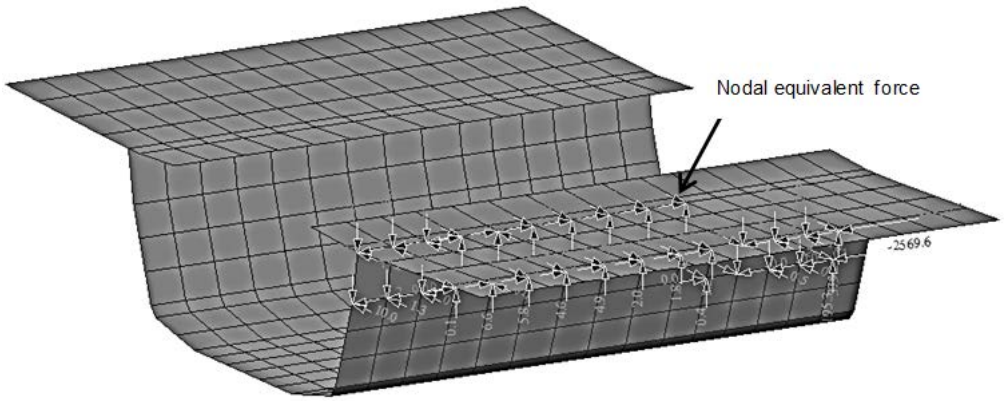

Fig. 9 Viaduct girder portion. Nodal equivalent forces of one tendon are displayed

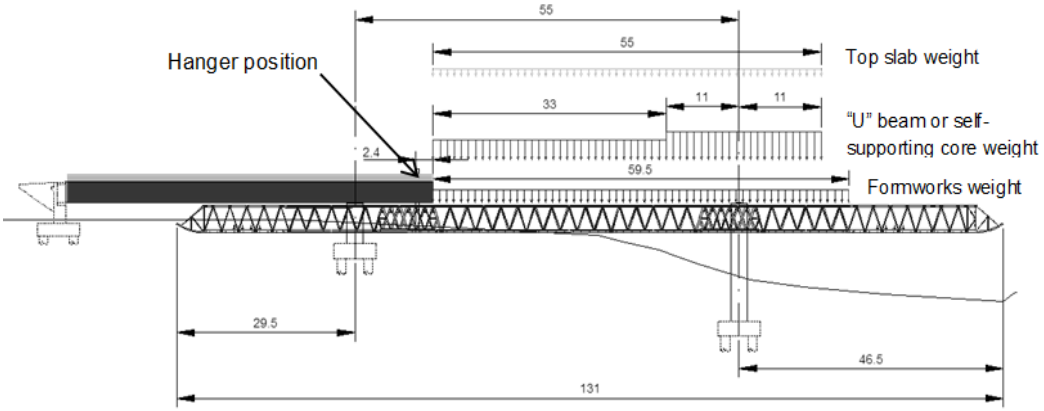

Fig. 10 Load scheme of the scaffolding

Tendon position at central sections of the deck was under the gravity centre of the section, to induce a negative moment in order to compensate the moment due to the permanent loads (Fig. 8).

3D models were constituted by standard Reissner-Mindlin shell elements of 0.5 m width×0.5 m length (Fig. 9). Shell elements were capable of taking into account in-plane and out-of-plane stresses. Variable thickness of bottom slabs and walls has been taken into account in 3D Finite Element (F.E.) models.

2.2 Material and prestressing characteristics

C35/45 concrete has been considered for numerical model because it is the most used concrete for road viaducts with a span between 50-60 m that have been built with MSS in Spain (Diaz de Teran *et al*. 2016). Tendon steel was Y 1860 S7. Bridge behaviour is very sensitive to rheological phenomena and constructive stages (Fiore *et al.* 2013, Bazant 1972, Kwak and Seo 2002, Kwak and Seo 2000, ACI committee 209 1997, Kasti 1990, Magura *et al.* 1964, Neville *et al.* 1983, Kwak and Son 2006, Ma *et al.* 2016, Siekierski 2016, Yang *et al.* 2015) so creep, shrinkage,

Table 2 Loads transmited to the front of the previous span by the scaffolding

	Q-2.4m (kN)
MSS self-weight Formwork weight	2295.1
1st casting phase weight	1365
Top slab weight (only transmitted in the traditional sequence)	1617.5

variation of compressive strength and relaxation have been taken into account in calculations of numerical models. Model Code 1990 (CEB-FIP 1990) has been considered to determine rheological parameters that have been considered for creep characterization: f_{ck}=35 MPa, Relative Humidity: 70%, "*h*": 336 mm and rapid hardening concrete: β_{SC}=8. Shrinkage was supposed to start from the first day because many of the structural elements start resisting the loads from this age.

Relaxation coefficient for prestressing tendons at 2D models has been set at 5% at infinite time. Matlab software has been used to obtain equivalent force for the 3D models to simulate prestressing forces. The values of the equivalent force came from 2D F.E. models; they have been computed in Matlab software, as explained at chapter 2.4, in order to determine punctual and distributed loads for 3D F.E. Models.

In order to determine the instantaneous prestressing losses some considerations were adopted as curvature friction factor μ=0.21, wobble friction factor K=0.00126, anchorage slip equal to 6 mm and elastic shortening.

2.3 Loads and boundary conditions

IAP-98 Code has been used to determine the loads and combinations (Ministerio de Fomento 1998).

The loads that have been considered were girder self-weight, dead loads, live loads, vehicular live load and loads that are transmitted by the scaffolding (Fig. 10). Combination of these loads as prescribed by IAPF code (Ministerio de Fomento 1998) has been considered to obtain the results of this paper:

a) Girder self-weight: 25 kN/m^3.

b) Dead loads:

• Pavement weight: 7 meters wide and 7 cm thick. Specific gravity: 23 kN/m^3.

• Sidewalk weight: 4.9 meters wide and between 10 and 23 cm thick. Specific gravity: 25 kN/m^3.

• Railing weight: load of 1.5 kN/m per each railing.

c) Live loads: 4 kN/m^2 placed at the worst positions.

d) Vehicular live load: consisted in 6 punctual loads of 100 kN, each one over a surface of 0.6×0.2 m^2. Transverse separation was 2 m and longitudinal separation was 1.5 m.

e) Scaffolding loads: the scaffolding transmited a punctual load 2.4 m behind the front of the last completed span (Fig. 10, Table 2):

External spans were supported by abutments and bents while internal spans were only supported by piers. Left extreme abutment was simulated considering constraints in X, Y, Z displacement and rotations at longitudinal axis (X axis). Right extreme abutment and piers were

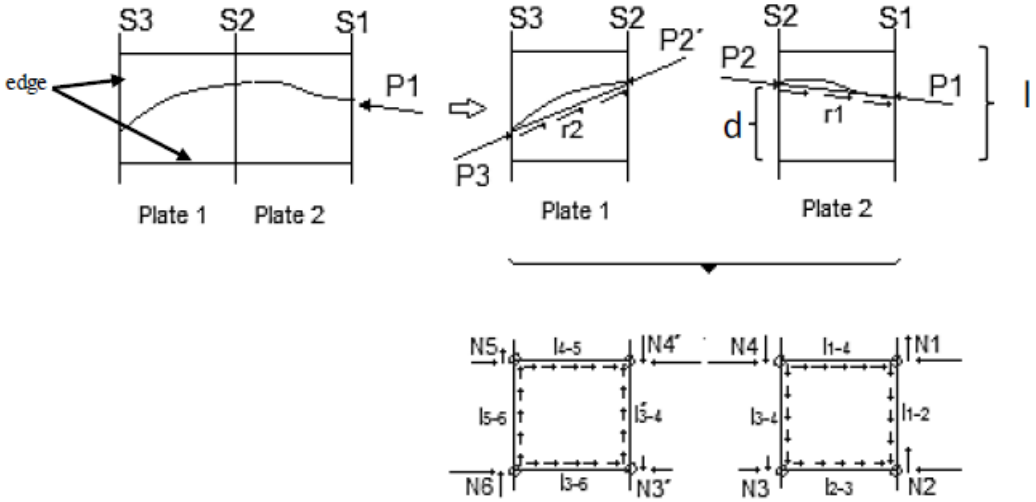

Fig. 11 Explanation of the conversion of tendon forces into equivalent loads

simulated considering constraints in Y and Z displacements and X axis rotations (Fig. 8).

New sequence, Solution 1 and Solution 2 have the advantage that the whole weight of the second casting phase is supported by the self-supporting core. On the other hand, the traditional constructive sequence implies that the interaction between the two parts, scaffolding and the first casting phase, must be taken into account in order to determine the percentage of the second casting phase that is supported by each part.

2.4 Prestressing force parameter

Prestressing load has been modelled as an equivalent tendon in 2D models (beam element models). Each span consisted in 8 tendons with an initial force of 6462.5 kN. The Midas Civil program divides a beam element into 4 segments and calculates equivalent forces for each segment. It is assumed that each tendon is linear at each segment. Midas Civil obtains forces at each end of the segments and distributes loads so that equilibrium can be established (Midas Civil 2011).

Matlab software was used to convert forces in tendons given by 2D F.E. models into equivalent punctual and distributed forces for 3D F.E. models. In case of 3D-models, prestressing forces were introduced as nodal and edge equivalent forces including the effects of creep, shrinkage and relaxation according to a procedure developed by the author and implemented in Matlab.

Software in Matlab took tendon forces from 2D Models for each stage and converted them into nodal and edge equivalent forces for shell elements in 3D Models (Fig. 11).

S_i represented the different sections at the 2D model. A tendon intercepted them at different coordinates and with different prestressing forces (P_i). The vertical dimension of the shell element was "*l*". The tendon crossed a shell element at a distance "*d*" from the lower node of the shell element. Orientation of P2 and P2' was determined by the straight line that linked the points where tendon entered and got out the shell element. The vertical and horizontal components of P_2 and P_2' were obtained by the sine and cosine of the angle that orientation line formed with horizontal axis. Nodal equivalent forces (N_i) depended on the distance between the point where the tendon crossed

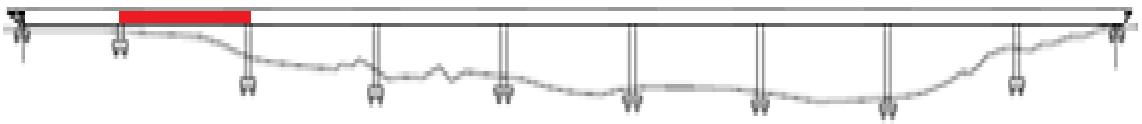

Fig. 12 Studied span: Span 2

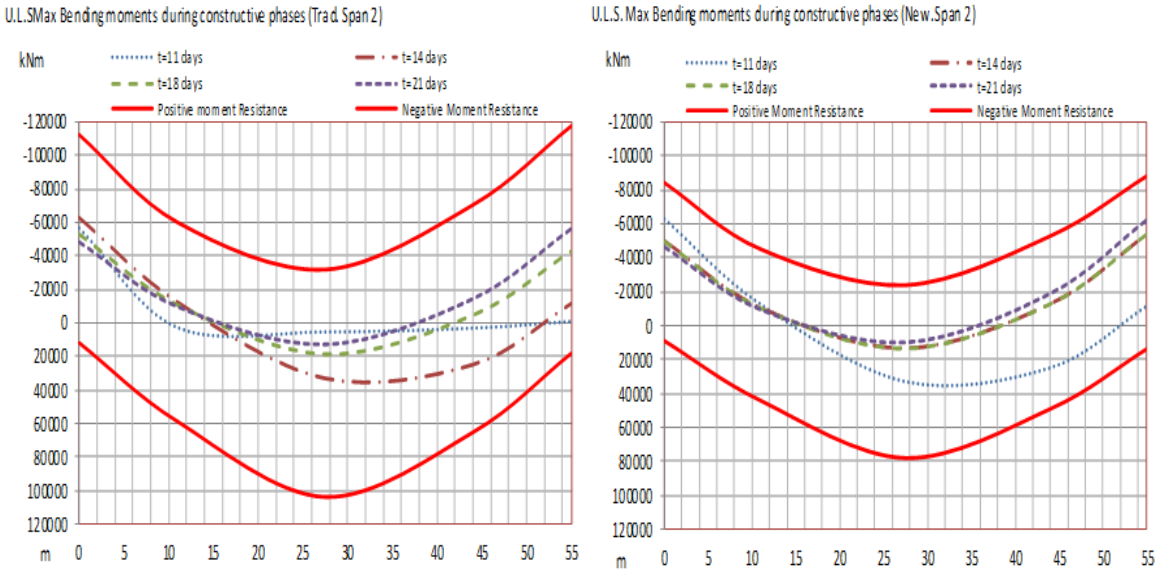

(a) Traditional sequence

(b) New sequence (75%)

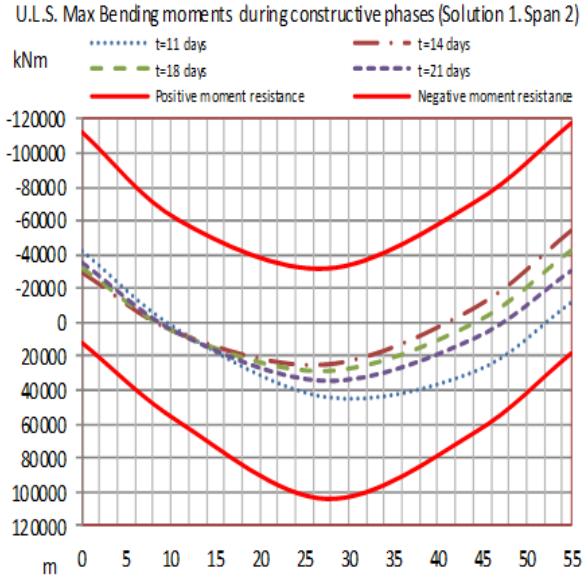

(c) Solution 1 (100%)

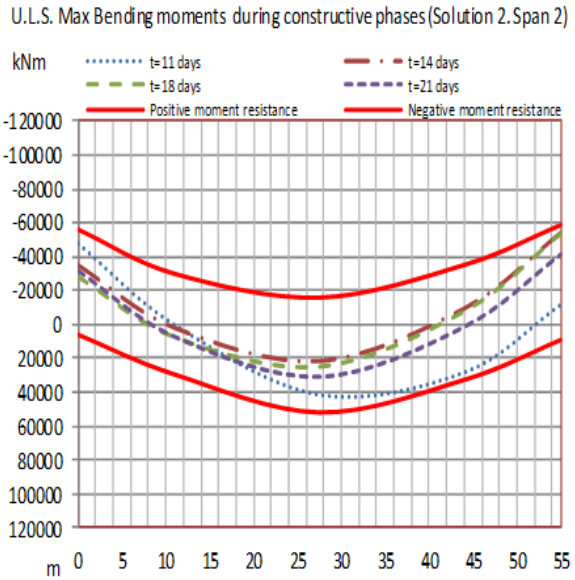

(d) Solution 2 (50%)

Fig. 13 E.L.U. Maximum bending moments of different sequences with different prestressing force percentage

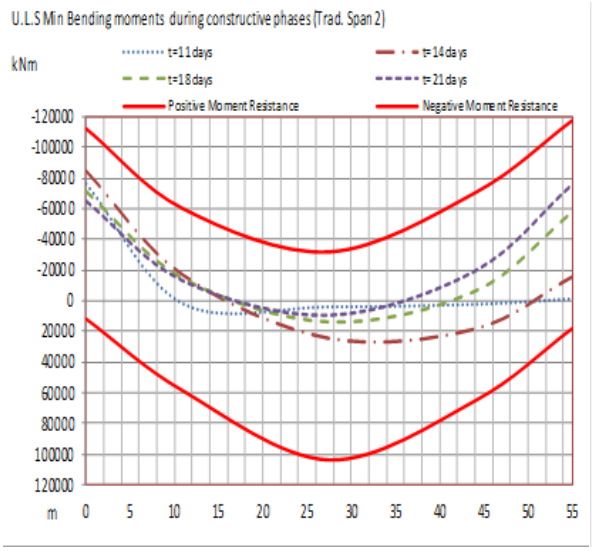

(a) Traditional sequence

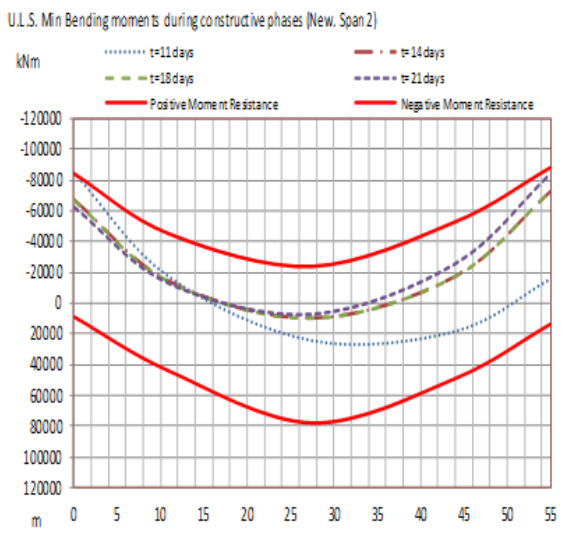

(b) New sequence (75%)

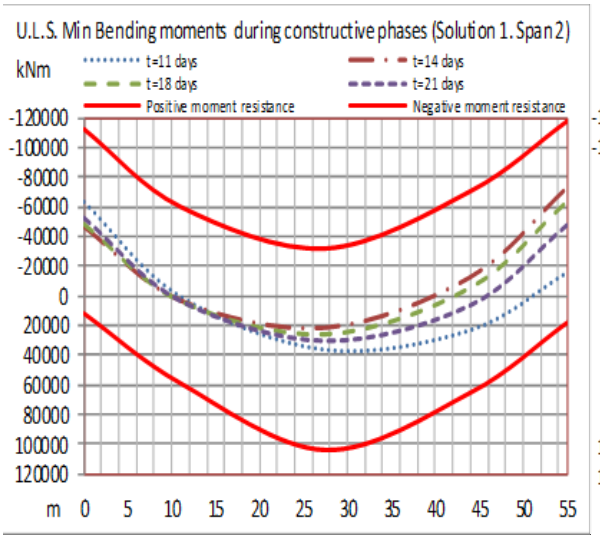

(c) Solution 1 (100%)

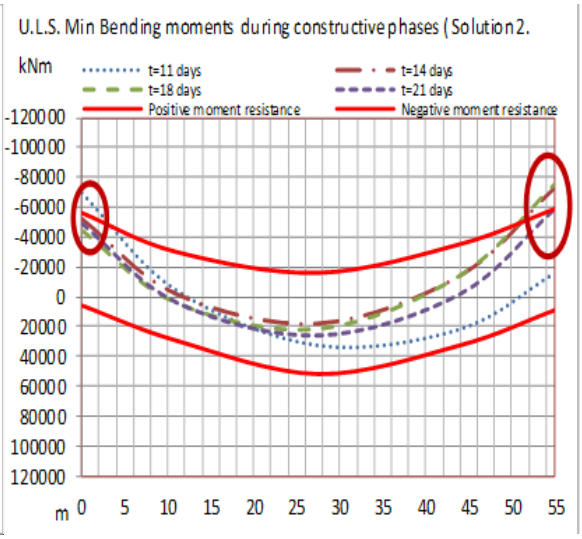

(d) Solution 2 (50%)

Fig. 14 E.L.U. Minimum bending moments of different sequences with different prestressing force percentage

the plate and the considered node of the shell. The closer the crossing point to the node, the higher the load that the node had: $N_4=P_2$ d/l, $N_3=P_2$ (l-d)/l (Fig. 11).

On the other hand, distribution of losses along the tendon was r_i. The equivalent tendon losses at shell elements were edge forces (I_{i-j}). As P_2' and P_3 values were different, losses could be determined. Edge forces values depended on the distance between the point where the tendon intercepted the shell and the shell edge length. When the tendon crossed the two opposite edges, the edge load was uniform and equal at both edges. It must be noticed that horizontal edges took the horizontal component of the lossess of the prestressing force and vertical edges took the

vertical component of the losses of the prestressing force (Fig. 11).

3. Results and discussion

Two different kinds of models have been performed, 2D models with beam elements and 3D models with shell elements. Numerical simulations were divided basically into four types of analysis in order to better explain the results:

a) 2D. Ultimate Limit State: bending moment global comparison at the second span (Fig. 12);
b) 3D. Ultimate Limit State: Internal forces at shell elements;
c) 3D-Service Limit State: stresses and crack opening in cross-section;
d) 3D-Service Limit State: transversal deformation.

3.1 2D. Ultimate limit state: Bending moment global comparison

Beam element models have been developed and bending moments in Ultimate Limit State combinations have been evaluated in this study. Negative and positive bending moment resistance for each constructive sequence has been calculated to improve the comparison.

Two main differences can be observed among the sequences at construction stages. The first difference affects the bending moments that is resisted by the section (continuous lines at Figs. 13 and 14). The bending moment resisted by the self-supporting core of the new sequence is lower (25-30%) than those resisted by the whole section of the traditional sequence. Solution 1 and the traditional sequence show quite similar bending moment resistance, whereas the Solution 2 shows the lowest bending moment resistance. The reason is that the traditional sequence and Solution 1 have 100% of the designed prestress when the section is not completed while the new sequence and solution 2 have 75% and 50% of those prestress, respectively, in the same construction stage. Moreover, the bending moment resistance at Solution 2 is insufficient to resist the actual moments at the sections over piers (Fig. 14) and additional passive reinforcement should be placed at these sections or an increase in girder height should be considered in order to resist negative bending moments.

The second difference regards values of the bending moments that the sequences present at the different stages during the construction (discontinued lines of the Figs. 13 and 14). These differences are due to the different static scheme evolution of the sequences (Diaz de Terán *et al.* 2016). At 11 days the moment that must be resisted by the traditional sequence is very low because at that age the girder is supported by the scaffolding. It can be noticed that at t=14 days the bending moment of the new sequence, solution1 and solution 2 over piles is greater (400%) than the traditional sequence. The reason is that the scaffolding is transmitting different weights. Although in both cases the MSS is supporting the weight of the first casting phase of the next span, this weight is not the same. In fact, the first casting phase of the traditional sequence is only formed by the lower slab and webs but the weight of the first casting phase of the new sequence is formed by the lower slab, webs and cantilevers of the top slab. The differences of bending moments at the other stages (t=18 days and t=21 days) are lower and can be explained by the static scheme of the structure. In this sense, while the whole section is resisting the weight of the span (and the scaffolding) at the traditional sequence, only the self-supporting core resists the weight at the new sequence, solution1 and solution 2. This difference of resisting sections implies a difference of stiffness at the structure and a differential distribution of the bending moments.

3.2 3D. Internal forces at shell elements

Shell models have been made in order to evaluate the Ultimate Limit State internal forces of each section of the viaduct. The shell elements of the section are numbered as follows (Fig. 15)

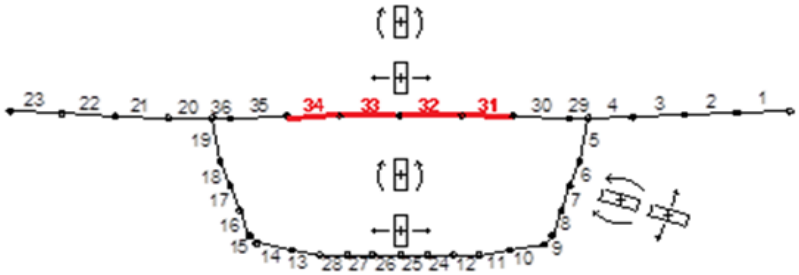

Fig. 15 Elements in a cross section (Central part of top slab in bold). Orientation of axial forces and bending moments

Table 3(a) Worst internal forces for construction stages at different sequences: Traditional sequence

Element	max Axial force (kN/m)	max Bending moment (kNm/m)	Bending moment min (kNm/m)	In plane shear force (kN/m)
1	1.1	0.0	-2.2	25.7
4	25.8	39.0	-94.6	1126.3
5	0.0	33.9	-88.8	4288.0
9	110.2	194.0	-74.7	2430.0
10	141.4	71.8	-74.6	1682.8
25	1294.1	56.1	-125.4	101.4
29	84.2	78.0	-76.5	1352.1
30	196.0	9.1	-41.9	799.2
31	511.5	10.7	-19.9	349.8

Table 3(b) Worst internal forces for construction stages at different sequences: New sequence (75%)

Element	Axial force max (kN/ml)	Bending moment max (kNm/m)	Bending moment min (kNm/m)	In plane shear force (kN/m)
1	8.1	0.0	-3.5	84.8
4	120.7	0.0	-124.2	1303.4
5	0.0	36.7	-112.3	4024.2
9	252.0	198.6	-199.9	2769.7
10	282.8	154.7	-199.6	1610.0
25	1269.8	172.2	-250.0	116.0
29	462.0	52.3	-55.3	937.6
30	458.6	7.4	-38.8	399.2
31	499.5	8.9	-13.0	303.0

Table 3(c) Worst internal forces for construction stages at different sequences: Solution 1 (100%)

Element	Axial force max (kN/m)	Bending moment max (kNm/m)	Bending moment min (kNm/m)	In plane shear force (kN/m)
1	10.0	0.0	-3.8	75.5
4	196.4	0.0	-132.9	1102.2
5	0.0	44.0	-90.1	4155.0
9	166.5	233.3	-178.5	2369.2
10	232.4	207.7	-177.1	1635.2
25	1084.1	206.4	-240.9	100.9
29	393.7	50.6	-52.7	1034.6
30	439.7	11.5	-39.5	445.4
31	496.5	8.2	-13.5	234.6

Table 3(d) Worst internal forces for construction stages at different sequences: Solution 2 (50%)

Element	Axial max (kN/m)	Bending moment max (kNm/m)	Bending moment min (kNm/m)	In plane shear force (kN/m)
1	12.9	0.0	-3.1	65.9
4	117.4	0.0	-99.5	1116.3
5	0.0	33.7	-95.3	2871.0
9	328.5	184.4	-201.6	2072.2
10	327.6	96.9	-199.3	1584.8
25	994.0	120.2	-246.4	138.6
29	365.2	60.3	-52.5	635.0
30	426.0	5.0	-39.0	334.2
31	486.0	8.1	-13.7	300.1

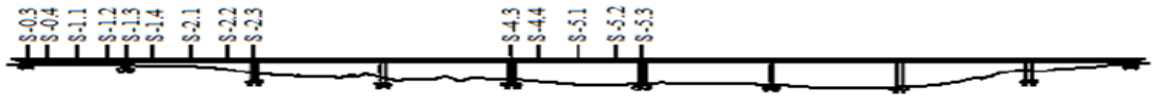

Fig. 16 Sections whose internal forces have been studied

Bending moments, axial forces and in-plane shear forces have been studied at the elements 1, 4, 29, 31, 5, 9, 10 and 25 as they are the midspan elements of the slabs or the connective elements between slabs and webs. The element 1 is at the edge of the top slab, the elements 4 and 29 are fixed to the web at the element 5. Elements 9 and 10 are at the joint between web and bottom slab. On the other hand, element 31 represents a mid-element of the top slab and element 25 represents the mid element of the lower slab. The worst values of internal forces among all stages are shown at Table 3. It should be pointed that the different column values represented at Table 3 are not concomitant nor placed at the same viaduct section. These values are the worst values at equivalent shell elements for the whole girder and all the stages.

The higher values of bending moments appear at the elements on the intersection of the slab

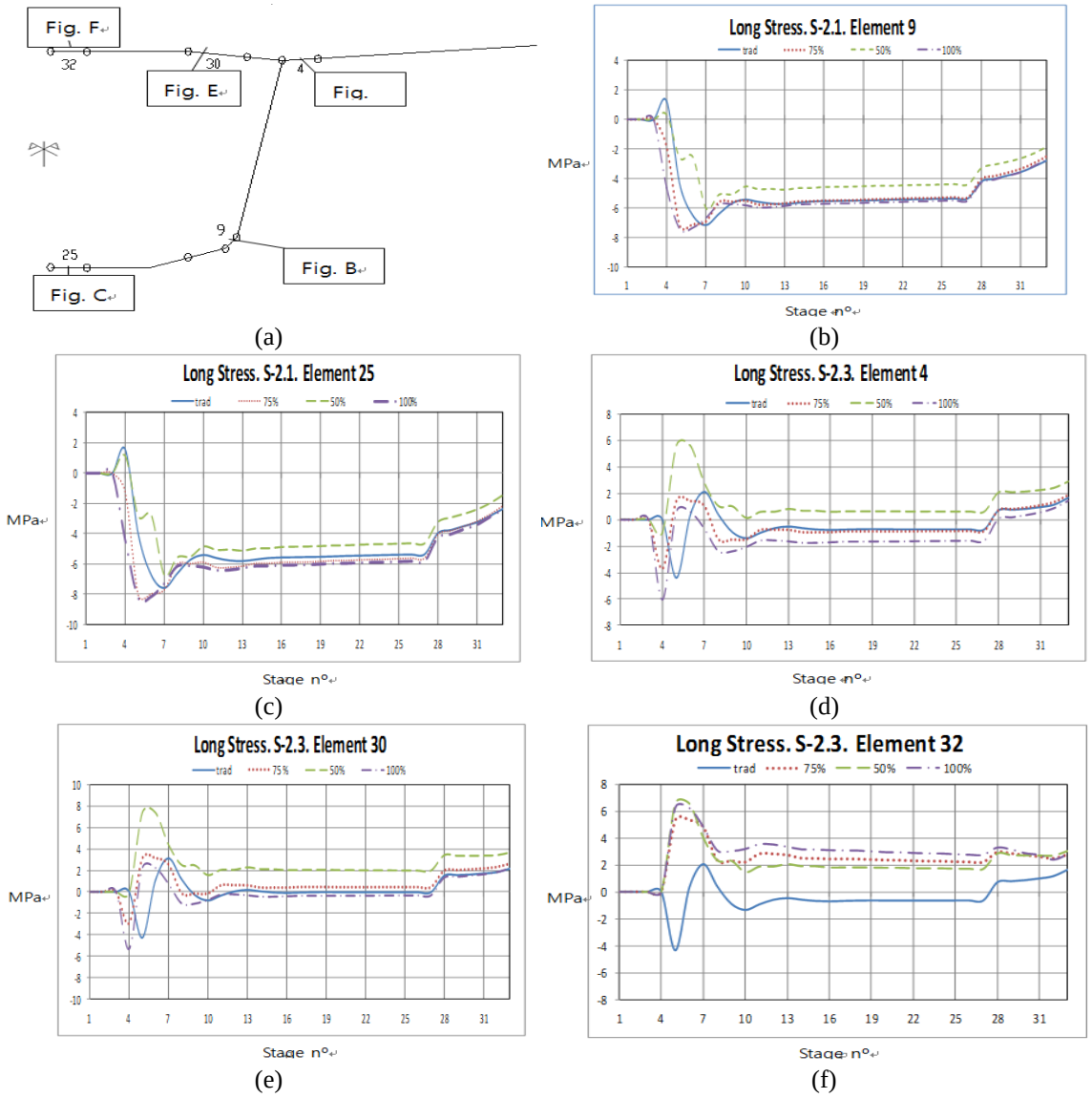

Fig. 17 Longitudinal stresses (MPa) at external fibers due to permanent loads at each stage. (+) tension. (-) compression

and webs (4, 5, 29, 9 and 10) and the centre of the lower slab. The main differences between the new sequence, Solution 1, Solution 2 and the traditional sequence in bending moments appear at the elements of the lower slab as values are 150% higher at the new sequence, solutions 1 and 2. This is due to the transverse deformation that the self-supporting core must resist at the new sequence, Solution 1 and Solution 2.

In-plane shear forces at the centre of gravity of shell elements are quite similar in all sequences except at the elements related to the casting joint of the new sequence (29 and 30). It can be observed that shear forces at the elements 29 and 30 at the new sequence, Solution 1 and Solution

2 are about 50% lower than at the traditional sequence. This difference is due to the fact that elements 29 and 30 are placed at the point of the section where the static scheme of the traditional sequence is different. This implies that elements 29 and 30 of the self-supporting core do not have to resist shear forces transmitted by the central part of the top slab when the self-supporting core is activated. It only receives these forces when the central part of the top slab is activated and new loads are acting over the structure.

If tension forces are considered, the main differences are related to the elements 9 and 10 on the intersection of the lower slab and webs (100% higher at the new sequence) and to the elements 29 and 30 that are placed at the casting joint of the new sequence, Solution 1 and Solution 2 (500% lower than the traditional sequence). The difference on the intersection of the lower slab and webs (elements 9 and 10) can be explained by the transverse deflection of the self-supporting core at the new sequence, Solution 1 and Solution 2. The section at the traditional sequence is completed and thus compressions are induced at elements 29 and 30. Otherwise, the new sequence as well as Solutions 1 and 2 do not have a completed top slab so none compression force can be induced at those elements.

The casting joint at the new sequence, Solution 1 and Solution 2 resists the higher values of internal forces that appear even if the worst values were considered as if they were concomitant (Díaz de Terán *et al*. 2013 a, b).

3.3 3D-service limit state: Stresses and crack opening in cross-section

The results that were obtained in this analysis correspond to 14 different sections in the viaduct (Fig. 16). Sections S-0.3, S-1.3, S-2.3, S-4.3, S-5.3 are placed over abutments or piers, sections S-0.4, S-1.4, S-4.4 are placed at 0.2 L at the right of the abutment or piers, sections S-1.1, S-2.1, S-5.1 are in the mid position of each span and sections S-1.2, S-2.2, S-5.2 are placed at 0.2 L at the left of each pier. The results until stage 27 are constructive stages: stage 1 corresponds to t=4 days, stage 2 corresponds to t=7 days, stage 3 corresponds to t=8 days, stage 4 corresponds to t=12 days, stage 5 corresponds to t=15 days and stage 6 corresponds to t=16 days. On the other side, stages 28 to 33 are the stages of the viaduct in service until t=10000 days, with live loads.

Tensile strengths of C35/45 concrete for different concrete ages are: $f_{ctm,3}$=1.9 MPa; $f_{ctm,7}$=2.5 MPa; $f_{ctm,28}$=3.2 MPa (CEB FIP 1990). They should be considered in order to analyse the crack opening possibility in S.L.S. while construction.

The differences between stresses at the sequences can be explained because the static scheme evolution of the sequences is different, as well as the distribution of stresses in order to resist the internal forces.

In case of longitudinal stresses at the lower slab of the central section S-2.1 (Figs. 17(b), (c)), the new sequence shows compressive stresses while the traditional sequence presents tensions at stage 4. The reason is that the self-supporting core of the new sequence has a section with less cross section area than the whole section of the traditional sequence. Moreover, the inertia of the self-supporting core is lower that the inertia of the whole section so the compressive stresses at the lower slab are greater at the new sequence. The Solution 1 lower slab at stage 4 is compressed because 100% of the prestressing force is introduced and compensates the effect of the self-weight. Otherwise, the Solution 2 lower slab at stage 4 is in tension because the prestressing force at that stage is only 50% of the final value and cannot compensate the self-weight.

In case of longitudinal stresses at the top slab of the section over pier S-2.3 (Figs. 17(d), (e), (f)), the traditional sequence presents a uniform distribution of tension values at the top slab

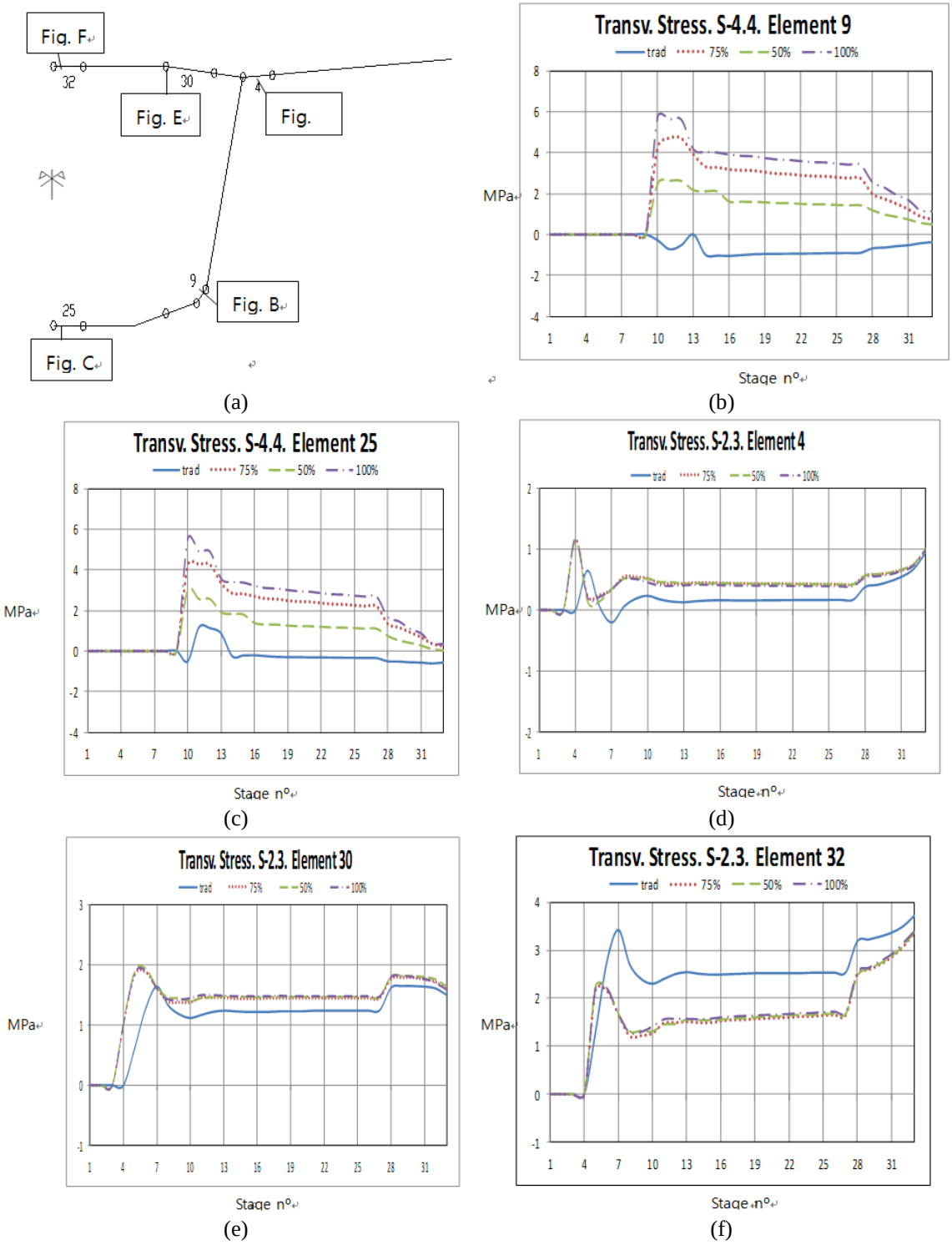

Fig. 18 Transversal stresses (MPa) at external fibers due to permanent loads at each stage. (+) tension. (-) compression

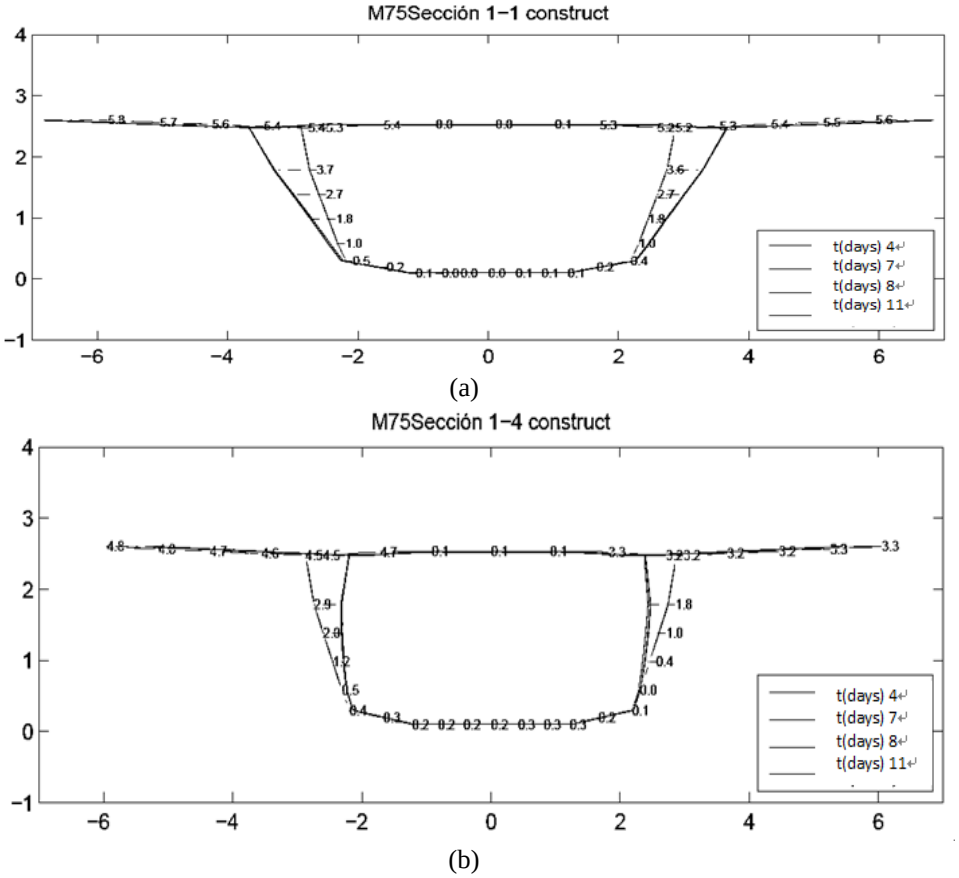

Fig. 19 New sequence. Maximum displacements (mm) at the new sequence. (a) mid-span section: S-1.1. (b) front of the deck: S-1.4

because the central part of the top slab is constructed since the first time the section is loaded and the stresses can be distributed uniformelly. These tensile values do not represent a problem in order to avoid concrete crack because the maximum value is 2.5 MPa for a concrete age of 7 days (stage 7) while the concrete strength at 7 days is also 2.5 MPa. On the other hand, the new sequence, the Solution 1 and Solution 2 do not present a uniform distribution of stresses at the top slab. The highest tensile longitudinal stresses at the top fiber over pier supports (S-2.3) appear at stages 5 and 6, which correspond to the scaffolding hanging from the front of the next span. The tensions induced by the scaffolding hanging are partially compensated by the prestressing force. The higher the prestressing force at the self-supporting core the lower the tensions at the top fiber as it can be seen when comparing tensions at Solution 1 (5.5 MPa) and Solution 2 (8 MPa) (Figs. 16(e), (f)). Tensile values at the new sequence, Solution 1 and Solution 2 require passive reinforcement.

Regarding transverse stresses at the lower slab of the section at 0.2 L at the right of piers S-4.4 (Figs. 18(b), (c)), the new sequence, Solution 1 and Solution 2 present higher transversal tensions at the lower fiber (6 MPa) than the traditional sequence (1.2 MPa) (Stages 10, 11 and 12) because the self-supporting core of the new sequence has a tendency to close at this position inducing

tensions at the lower slab. The value of tensions at the new sequence (4.3 MPa) is much higher than the concrete strength at 3 days (1.9 MPa) and the new sequence requires passive reinforcement in order to limit the crack opening.

The new sequence, Solution 1 and Solution 2 present similar results for the element 32 (2.2 MPa) than the traditional sequence (3.4 MPa) when transverse stresses at the top slab over piers (S-2.3) are compared, see Figs. 18(d), (e), (f)). The reason is that the section of the girder over piers has the tendency to open. At the traditional sequence, the central part of the top slab is already constructed and stops this tendency, generating tensions. The other sequences do not have the central part of the top slab already constructed at the equivalent stage and, when it is constructed afterwards, tensions do not appear.

3.4 3D-service limit state: Transversal deformation

The transversal deflection is only taken into account for the new sequence because the traditional sequence cross section is completed when the span is loaded. Regarding the first span, the midspan section opens 11.7 mm at the new sequence. Otherwise, the front-span section closes 7.7 mm (Fig. 19). Differences between the new sequence, Solution 1 and Solution 2 are minimum (1 mm) so it can be concluded that the self-weight of the first casting joint is the main effect to explain the transversal deflection. However, the prestressing force influence on the transverse deflection is quite small.

If tolerance considerations are made in order to construct the second casting phase of the section, the transverse deflection is not an issue. If the opening displacement of the central section (6.5 mm) is added to the closing displacement at the front of the deck (4.5 mm), a total value of 11 mm is obtained. Tolerance is high as the second casting phase needs a minimum casting joint of 35-40 cm width in order to allow the loop joint length. Otherwise, for the new sequence, Solutions 1 and 2, especial considerations should be made in order to avoid issues regarding vertical displacements of cantilever tips, transverse inclination of the top slab and final profile of parapets, although they have been negligible for bridges constructed up to date with the new sequence (Diaz de Teran *et al.* 2016).

4. Conclusions

Regarding the main issues related to the new sequence that have been compared to the traditional sequence, Solution 1 and Solution 2 these conclusions can be presented:

• Comparison of global bending moments of the girder (2D. Ultimate Limit State): though bending moments present different values at equivalent constructive stages, the most critical factor is due to the reduction of the section strength (-30%) because of the lower percentage of active steel (75% of total) when the self-supporting core is activated at the new sequence.

• If internal forces are compared (3D. Ultimate Limit State), the new sequence presents higher bending moments at the lower slab, as well as higher axial forces and lower shear forces at the elements that correspond to the casting joint of the new sequence, Solution 1 and Solution 2. This is due to the different static scheme evolution.

• If stresses are compared (3D. Service Limit State), a conclusion about which sequence shows lower values of tensions cannot be made, because the traditional sequence has lower values of longitudinal tensions but some transverse tensions are higher than the new sequence and Solutions

1 and 2.

• The transverse deformation of the self-supporting core is limited at 11.5 mm and is not a critical factor in order to be taken into account for designing.

Solution 1 and Solution 2 represent an improvement in relation to the new sequence as they imply only one prestressing shift at each span. The Solution 1 does not imply worse internal forces including the casting phase nor much worse stresses at the sections that should be considered regarding crack opening. The only stress value that is clearly higher than at the new sequence is the transverse tension at the top slab. Hence, additional passive reinforcement is required to control crack opening. Moreover, transverse deflection conditions are quite similar to that at the new sequence. It implies that Solution 1 is a simpler and cheaper sequence to be considered in order to achieve a constructive improvement of viaducts with movable scaffolding system (MSS).

Solution 2 is also an available constructive sequence but it is limited due to the substantial losses of prestressing force that are likely to occur for very long tendons applied through two spans. Thus, the active reinforcement is not enough to resist Ultimate Limit State during construction, so negative bending moments on piers during construction require additional passive reinforcement to resist them or an increase of the girder height.

References

ACI Committee 209 (1997), "Prediction of creep, shrinkage and temperature effects in concrete structures", ACI 209 R-92, American Concrete Institute Detroit.

Bazant, Z.P. (1972), "Prediction of creep effects using age-adjusted effective modulus method", *ACI J.*, **69**, 212.

Bojidar, Y. (2015), "Joints: The weak link in bridge structures and lifecycles", *Wind Struct.*, 1**5**(3), 543-553.

Comité Euro-International du Béton (2008), *CEB-FIP Model Code 1990*, Thomas Telford Ltd.

Council (1989), "Council directive 89/391/EEC of 12 June 1989 on the introduction of measures to encourage improvements in the safety and health of workers at work", *Official J.*, L183, 0001-0008.

Council (1992), "Council directive 92/57/EEC of 24 June on the implementation of minimum safety and health requirements at temporary or mobile construction sites", *Official J.*, L245, 0006-0022 .

Daebritz, M. and Lee, M. (2010), "Span by span movable scaffolding systems", IABSE WG 6, State of Art of Bridge Deck Erection, Safe and Efficient Use of Special Equipment, Singapore.

Demmel, J.W., Gilbert, J.R. and Li, X.S. (1999), "An asynchronous parallel supernodal algorithm for sparse Gaussian elimination", *SIAM J. Matrix Analys. Appl.*, **20**(4), 915-952.

Díaz de Terán, J.R., Haach, V.G., Turmo, J. and Jorquera, J.J. (2016), "Improved construction of concrete viaducts with movable scaffoldinf systems in Spain", *J. Bridge Eng.*, 04016050.

Díaz de Terán, J.R. (2013), "New constructive procedure of viaducts with movable scaffolding system and new evolutive sequence", Ph.D. Dissertation, Universidad Politécnica de Cataluña, Barcelona.

Diaz de Teran, J.R., Turmo, J., Jorquera, J., Barragan, B., Ramos, G. and Aparicio, A. (2013a), "Optimization of in situ construction of concrete decks: Flexure tests of compact splices of reinforcement between phases", *Constr. Build. Mater.*, **41**, 191-203.

Diaz de Teran, J.R., Turmo, J., Jorquera, J., Barragan, B., Ramos, G. and Aparicio, A. (2013b), "Shear-off strength of compact reinforcement for improved splicing site construction of concrete structures", *Constr. Build. Mater.*, **47**, 199-207.

Duff, I.S. and Reid, J.K. (1984), "The multifrontal solution of unsymmetric sets of linear equations", *SIAM J. SCI Stat. Comput.*, **5**(3), 633-641.

Fiore, A., Foti, D. and Monaco, P. (2013), "An approximate solution for the rheological behavior of non-homogeneous structures changing the structural system during the construction process", *Eng. Struct.*, **46**, 631-642.

Kasti, F.A. (1990), "Nonlinear material and time dependent analysis of segmentally erected reinforced and prestressed concrete composite 3D frame structures", Report No. UCB/SEMM 90-03, University of California, Berkeley, U.S.A.

Kwak, H.G. and Son, J. (2006), "Determination of design moments in bridges constructed with a movable scaffolding system (MSS)", *Comput. Struct.*, **84**(31), 2141-2150.

Kwak, H.G. and Seo, Y.J. (2000), "Long-term behavior of composite girder bridges", *Comput. Struct.*, **74**(5), 583-599.

Kwak, H.G. and Seo, Y.J. (2002), "Numerical analysis of time-dependent behavior of pre-cast pre-stressed concrete girder bridges", *Constr. Build. Mater.*, **16**(1), 49-63.

Leonhardt, F. (1994), *Brücken /Bridges*, 4th edition, Stuttgart: Deutsche Verlags-Anstalt.

Liu, J.W.C. (1992), "The multifrontal method for sparse matrix solution: Theory and practice", *SIAM Rev.*, **34**(1), 82-109.

Ma, Y., Wang, Y., Su, Y. and Mei, S. (2016), "Influence of creep on dynamic behavior of concrete filled steel tube arch bridges", *Steel Compos. Struct.*, **21**(1), 109-122.

Magura, D.D., Sozen, M.A. and Siess, C.P. (1964), "A study of stress relaxation in prestressing reinforcement", *J. PCI*, **9**(2), 13-57.

Midas Civil (2011), "Civil 2011. On line manual", March 4, 2012.

Ministerio de Fomento (1998), "Instrucción de Acciones en Puentes. Intruction of loads in bridges", Ministerio de Fomento, Madrid.

Neville, A.M., Dilger, W.H. and Brooks, J.J. (1983), *Creep of Plain and Structural Concrete*, Const. Press, London.

Pacheco, P., Coelho, H. and Borges, P. (2011), "Technical challenges of large movable scaffolding systems", *Struct. Eng.*, **21**(4), 450-455.

Pacheco, P., Fonseca, A., Resende, A. and Campos, R. (2009), "Sustainability processes in bridge construction process", Reviewed October 26, 2010, Springerlink: www.springerlink.com.

Sadeghi, J. and Rezvani, F.H. (2013), "Development of non-destructive method of detecting steel bars corrosion in bridge decks", *Struct. Eng. Mech.*, **46**(5), 615-627.

Shin, D.H., Chung, C.H., Oh, C.H., Park, S.J., Kim, I.G., Kim, Y.J., Byun, T.K. and Kang, M.G. (2016), "Structural behavior of precast concrete deck with ribbed loop joints in a composite bridge", *Smart Struct. Syst.*, **17**(4), 559-576.

Siekierski, W. (2016), "Analysis of concrete shrinkage along truss bridge with steel-concrete composite deck", *Steel Compos. Struct.*, **20**(6), 1237-1257.

Yang, M.G., Cai, C.S. and Chen, Y. (2015), "Creep performance of concrete-filled steel tubular (CFST) columns and applications to a CFST arch bridge", *Steel Compos. Struct.*, **19**(1), 111-129.

Zwicky, D. (2013a), "Bond and ductility: A theoretical study on the impact of construction details-part 1: basic considerations", *Adv. Concrete Const.*, **1**(1), 103-119.

Zwicky, D. (2013b), "Bond and ductility: A theoretical study on the impact of construction details-part 2: structure-specific features", *Adv. Concrete Const.*, **1**(2), 137-149.

CC